www.czasopisma.pan.pl PAN POLSKA AKADEMIA NAUK www.journals.pan.pl

Arch. Metall. Mater. **66** (2021), 2, 601-608

DOI: 10.24425/amm.2021.135897

M. PAĆKO[1], J. KRAWCZYK[1], T. ŚLEBODA[1], Ł. FROCISZ[1],
M. RUMIŃSKI[1*], O. LYPCHANSKYI[1], T. TOKARSKI[1], P. PIASECKI[2]

STATE OF STRAIN AND DEVELOPMENT OF MICROSTRUCTURE OF 22MnB5 STEEL AND Al-Si COATING DURING DEEP DRAWING OF AUTOMOTIVE B PILLAR

The analysis of the development of the microstructure of deep drawn automotive B pillar, as well as the analysis of deformation based on numerical simulation and experiment, was performed. The microstructure of steel sheet as well as Al-Si coating after various stages of B pillar production was investigated. It was found that the obtained microstructure of the B pillar was significantly different from that described in many studies as a proper one. The microstructure of the investigated material consisted of martensite, bainite, and a small amount of ferrite. Al-Si coating, despite its morphological changes, remained on the surface of B pillar and, in spite of this, did not fully eliminate oxidation and decarburization of B pillar material. The analysis of the state of strain allowed to evaluate the deformation safety of the process, as well as to verify the simulation results through measurements of sheet thickness variations.

Keywords: B pillar, 22MnB5 steel, aluminide coating, deep drawing, hot stamping

1. Introduction

The application of high strength steel is necessary for ensuring the reduction of the total weight of the vehicle as well as for the improvement of crashworthiness and passengers' safety. Boron steels are widely used in the automotive industry because they fulfill these requirements. Such steels are processed by deep drawing, a process patented by Swedish company „Plannja" in 1977. The first producer that applied boron steel in mass production was Saab. In 1984 Saab Automobile AB applied such steel for parts used in Saab 9000. In 1987 three million automotive parts were produced from boron steel. By 2007 this number increased to 107 million parts produced each year [1]. Currently, deep drawn boron steel is applied for: front and rear bumper beams of a car, door reinforcement, vertical strengthening of front car window, B pillar, car roof, and floor strengthening parts, cross-beams of car dashboard and cross-beams of car roof [1]. The widely used method of forming those automotive parts is hot stamping. Together with the increasing demands of the automotive industry, this method gained more and more recognition. Nowadays hot forming (HF) technology is developing very intensively (210 million deep-drawn parts in 2015) and finds wider and wider application in the manufacturing of structural components of self-supporting car bodies, replacing other technologies and materials [2]. There are much research works aimed at further development of hot stamping technologies for production of structural parts having more and more attractive mechanical properties [3,4]. The analysis of the microstructural, technological and mechanical aspects are essential for the optimization of hot stamping technology. One of the most important problems is the optimization of the geometrical design of cooling systems of hot stamping tools [5]. The selected research works concern such problems as the application of tailored tempering process, in order to create regions of the part showing different strength-ductility combinations [6,18], modelling of microstructure evolution with the development of new models [7], the analysis of microstructure and formability of the applied Al-Si coatings [8], the influence of asymmetric pre-rolling and pre-heating operations on the evolution of microstructure [9] or the effect of boron microalloying on microstructure and mechanical properties of hot-stamped steel [10]. The effects of phase transformation are considered essential when developing a suitable model for the simulation of a hot stamping process [11]. A great number of the research works are aimed at optimization of the process of the production of B pillar. For example, Liu et al. [12] report that the proper selection and development of hot stamping production

[1] AGH UNIVERSITY OF SCIENCE AND TECHNOLOGY, AL. MICKIEWICZA 30, 30-059 KRAKOW, POLAND
[2] KIRCHHOFF AUTOMOTIVE, MIELEC, POLAND

* Corresponding author: ruminski@agh.edu.pl

system (forming dies, type of press, heating equipment, conveying system, and production line control system) is essential from the point of view of resulting mechanical properties of a final product. Min et al. [13] investigated the influence of pre-forming applied in the indirect hot stamping method on phase transformation behavior of boron steel. A more comprehensive study on the concept of hot stamping, including the discussion of process design, quality control, tool fabrication, process simulation, and future outlooks, is provided in [14]. Bok et al. [15] applied and compared different empirical phase transformation models, coupled with finite element method (FEM) thermo-mechanical simulation, in order to predict the mechanical properties of a product. In particular, the researchers analyze new processes, e.g. warm stamping of the third generation medium-Mn steel [16,17], the potential of cryogenic forming [19] or the effect of contact pressure on heat transfer coefficient between the steel blank and die and the formability of hot-formed B pillar [20]. This research is focused on the analysis of the microstructure of steel and protective coating of B pillar manufactured by hot stamping, as well as the analysis of deformation of steel sheet during forming.

2. Material and methods

2.1. Material

22MnB5 steel sheet was used for forming of B pillar. The chemical composition of steel is given in Table 1. In as-received condition, the microstructure of this steel consisted of ferrite and spheroidite precipitations (Fig. 1). The microstructure presented in Fig. 1 shows that the initial material is in the annealed state. Before stamping steel sheet was covered with a protective coating. The morphology of this coating along with a map of chemical elements distribution is shown in Fig. 2. In the first area numerous pores causing structural discontinuity can be noticed (Fig. 2a, b). The diffusion layer consists mainly of Al (Fig. 2f), Fe (Fig. 2d) and Si (Fig. 2e). In spite of defects existing in the coating, it can be expected that it should keep its protective properties during the deep drawing process.

TABLE 1

Chemical composition (wt. %) of 22MnB5 steel used in the investigation

C	Mn	P	S	Si	B	Al	Cr	Ti	Cu	Ni	Fe
0.23	1.18	0.014	0.001	0.27	0.003	0.04	0.19	0.04	0.02	0.02	Bal.

2.2. B pillar forming process and method of sampling for the investigations

In this research, the steel sheet was subjected to hot deep drawing. The investigated part was austenitized at 900°C for 5 minutes. According to work [1] such temperature and time of austenitizing guarantee austenitic microstructure in deep drawn steel. After deformation, the parts of deep drawing press do not move apart to enable the hardening of the deep-drawn part. Processed material is hardened by water flowing through special channels in the head of the press. Achieving a martensitic microstructure requires an appropriate cooling rate. For 22MnB5 steel, the minimum cooling rate is 27°C/s. If this cooling rate is not achieved, the microstructure of the processed material may not be fully martensitic. The application of a water-cooled stamp should additionally ensure an appropriate cooling rate over the entire length of the deep-drawn part. However, due to the complexity of the shape of the drawn part, some differences in the cooling rate may occur in some sections of the B pillar.

The forming process, as well as the assembly of a stamping die used in the manufacturing of B pillar, are shown in Fig. 3. In the first stage, a punch exerts pressure on the upper surface of a drawing piece, causing the deformation and holding the material at the same time. Further movement of tools results in pressing the material between the blank holder and the end faces of trimming cutters. In the next stage, the die surfaces are engaged to form lateral surfaces of a drawing piece. The material, while being deformed by deep drawing, is held down by the blank holder at the same time. This is a critical stage, due to the risk of wrinkling. The selection of the optimum blank holder force is crucial, since the excessive pressure may lead to over-thinning or a fracture of a steel sheet. In the last stage, the excess material is trimmed.

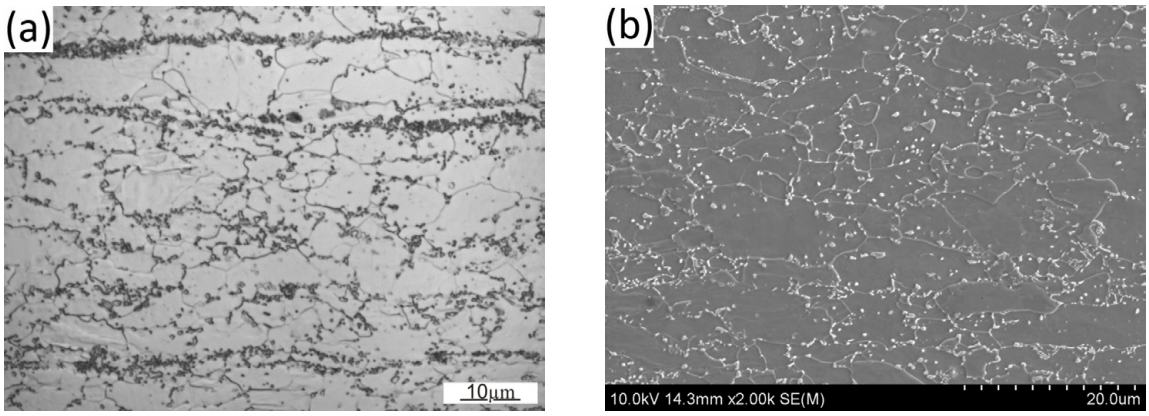

Fig. 1. Microstructure of steel sheet before deep drawing: (a) light microscopy; (b) scanning electron microscope (SEM), etched with 2 % nital

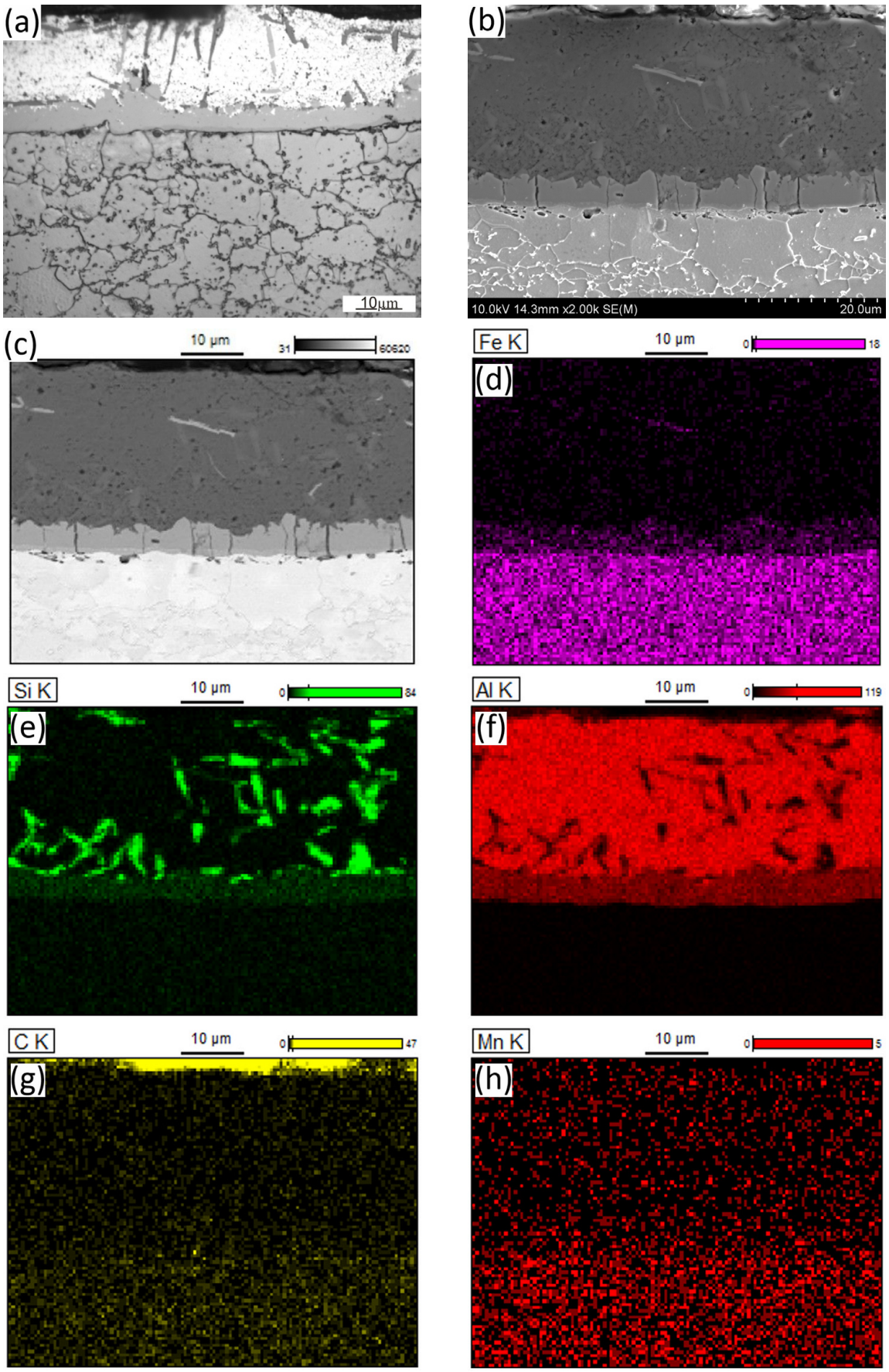

Fig. 2. Morphology of protective coating on steel sheet before deep drawing: (a) light microscopy; (b) SEM – secondary electron detection; (c) SEM – backscattered electron detection; (d) Fe distribution for the area shown in Figure (c); (e) Si distribution for the area shown in Figure (c); (f) Al distribution for the area shown in Figure (c); (g) C distribution for the area shown in Figure (c); (h) Mn distribution for the area shown in Figure (c)

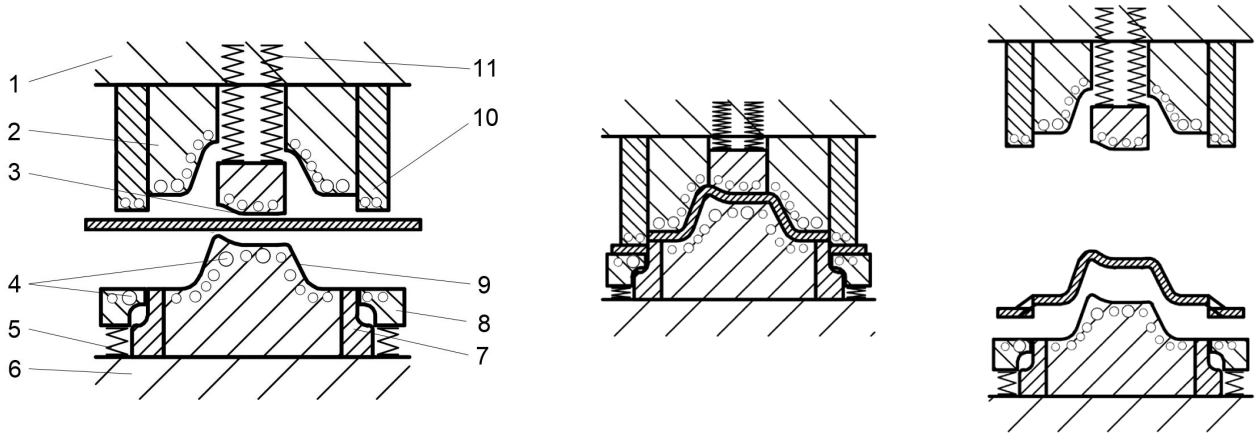

Fig. 3. Tools arrangement and stages of B pillar forming process (1 – top plate, 2 – upper die, 3 – punch, 4 – cooling channels, 5 – blank holder spring, 6 – bottom plate, 7 – lower trimming cutter, 8 – blank holder, 9 – lower die, 10 – upper trimming cutter, 11 – punch spring)

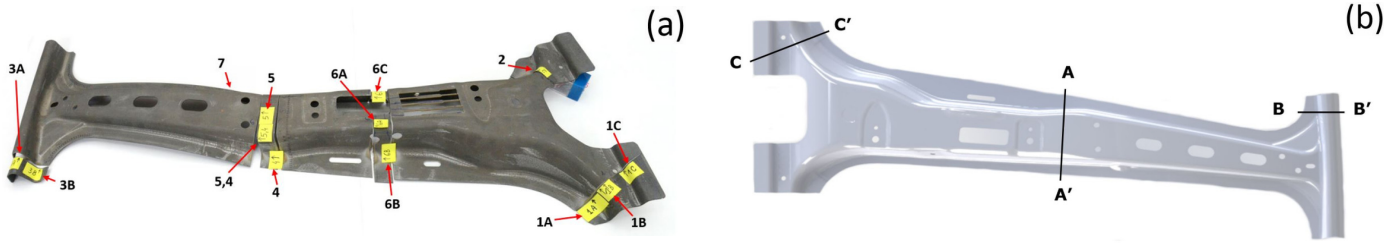

Fig. 4. The method of sampling and marking the samples for the investigations (a) and locations of thickness measurements (b)

Fig. 4 presents the B pillar prepared for sampling. The method of marking the samples, as well as the locations of sheet thickness measurements, is also shown in Fig. 4.

2.3. Numerical modelling

According to the deep drawing process described above, the assembly of tools was prepared for the simulation using Pam-Stamp 2G software. The geometrical models of tools created based on the draw piece model are shown in Fig. 5, with the process parameters, also specified.

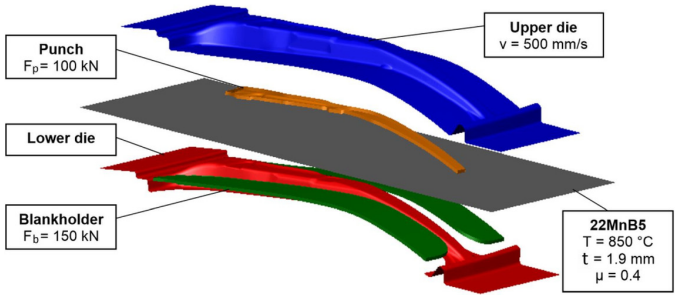

Fig. 5. Tools assembly and process parameters applied in the numerical simulation using Pam-Stamp 2G software

The mechanical properties of 22MnB5 steel are specified in the program's materials library. In the simulation, the material's transition to plastic state is described according to the Hill48 yield criterion (Eq. (1)). This criterion describes the yielding of orthotropic materials, i.e. those which show anisotropy of mechanical properties. It is most often applied to sheet and strip forming processes, where plane and normal anisotropy occurs.

$$\sigma_{Hill48} = \sqrt{\frac{1}{2}\left[\begin{array}{l} H\left(\sigma_{11}-\sigma_{22}\right)^2 + F\left(\sigma_{22}-\sigma_{33}\right)^2 + \\ +G\left(\sigma_{33}-\sigma_{11}\right)^2 + 2N\sigma_{12}{}^2 \end{array}\right]} \quad (1)$$

where H, F, G, and N are coefficients characterizing the yielding of a material.

In case when F = G = H = 1 and N = 3, then the equation describes isotropic material. Considering the lack of published data on plastic strain ratios for 22MnB5 steel, the isotropic material model was employed. The process simulation assumed isothermal conditions, with the temperature of a material $T = 850°C$. The heat exchanges with tools and environment, as well as phase transformations, were not taken into consideration, thus significantly reducing the time of calculations.

3. Results and discussion

3.1. Metallographic analysis

The morphology of protective coating after hot deep drawing is shown in Fig. 6. It can be noticed, that protective coating still exists on the surface of the analyzed part (Fig. 6a). How-

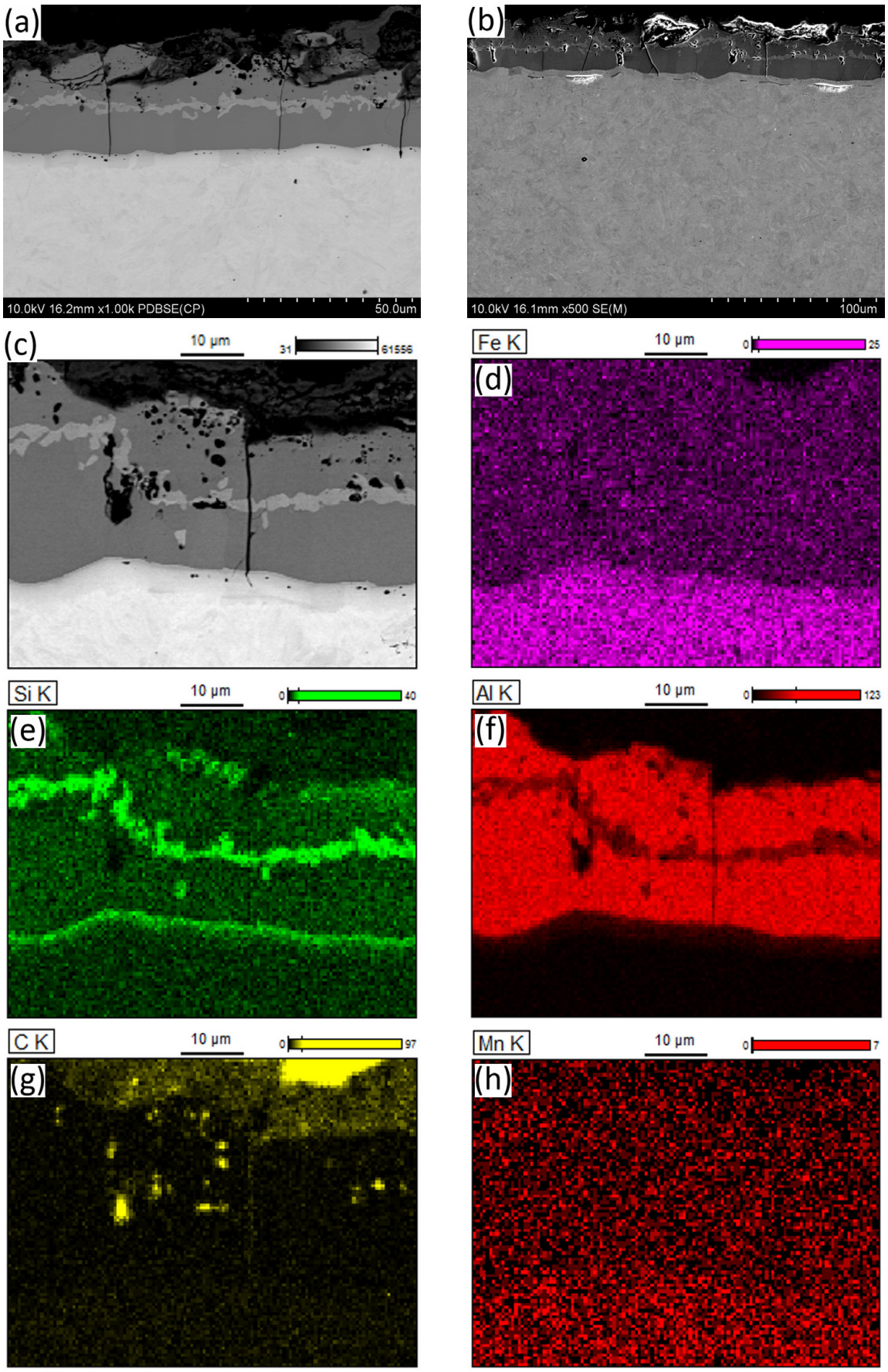

Fig. 6. Morphology of protective coating on steel sheet after deep drawing: (a) SEM – backscattered electron detection; (b) SEM – secondary electron detection; (c) SEM – backscattered electron detection; (d) Fe distribution for the area shown in Figure (c); (e) Si distribution for the area shown in Figure (c); (f) Al distribution for the area shown in Figure (c); (g) C distribution for the area shown in Figure (c); (h) Mn distribution for the area shown in Figure (c)

ever, the microstructure of this coating underwent substantial changes (Fig. 6a-c compared to Fig. 2a-c). The main difference concerns the appearance of a porous external layer consisting of oxides (Fig. 6b). Next, the porous metallic layer can be observed (Fig. 6a,c). This layer is free from precipitations and is separated from other layers having a different chemical composition (Fig. 6a,c). Grain boundaries and cracks proceed through that layer to the end of that layer (Fig. 6a-c). Subsequently, a thin intermediate layer can be noticed, under which thin decarbonized layer (most probably ferritic) exists (Fig. 6c). Under that layer, some porosity can be observed (Fig. 6a-c).

The maps of the distribution of the chemical elements in protective coating and in surface layer of the drawn part were analyzed (Fig. 6c-h). This analysis shows, that the external layer mainly consists of iron oxides (Fig. 6c compared with Fig. 6d). The iron content distribution suggests that intense diffusion of iron through protective coating took place during heating up the steel sheet before stamping and during the forming stage (Fig. 6d compared to Fig. 2d). Silicon diffused into three areas (Fig. 6e): external area of the metallic layer (under the layer of oxides); intermediate area, forming parallel to the surface of steel sheet layer rich in silicon and separating two layers rich in Al (Fig. 6f); area of thin layer separating layer rich in Al from the base material layer rich in Fe. Under that layer the area with high Fe content and low C content exists (decarbonized ferritic layer) (Fig. 6g). It can be stated, that the applied coating only restricted the oxidation of iron and decarburization of steel sheet, despite the fact that it remained on the surface of the steel sheet. Such a statement is confirmed by the observed diffusivity of iron through the protective coating. However, the changes in protective coating characteristics may have a disadvantageous influence on further production processes like for example painting.

The microstructure of the investigated material was martensitic (with probable small amount of lower bainite) with a small amount of ferrite (Fig. 7).

Ferrite content was evaluated in the samples taken from deep drawn parts (Fig. 8). 10 estimations were performed for each sample applying a grid with 441 nodes. It can be noticed, that higher content of ferrite exists in the flange of the pillar than in the middle section of this pillar. It can be explained by a need for a reduction of the mechanical properties of the pillar flange due to its greater dimensions comparing to more narrow parts of the pillar. It brings profitable effects connected with the optimization of the mechanical performance of the pillar and car body.

Hardness measurements were carried out in the areas of the microstructural analysis to confirm this thesis (Fig. 9). It can be noticed, that the average hardness of the pillar flange is only slightly lower than the average hardness of its middle section. Different relationships can be noticed considering the correlation between hardness and ferrite content, with respect to the middle section of the pillar and to the samples taken from the pillar flange (Fig. 10). It can be assumed, that in this case the amount of ferrite may be connected with the amount of strain. Higher strains facilitate diffusion transformations (also ferrite nucleation) during cooling from austenitic range. It should, however, be noticed, that hardness is influenced by many other factors: the extent of dynamic recrystallization, the influence of grain size on the hardenability, local fluctuations of the chemical composition. Additional research should be realized in order to determine the existing relationships.

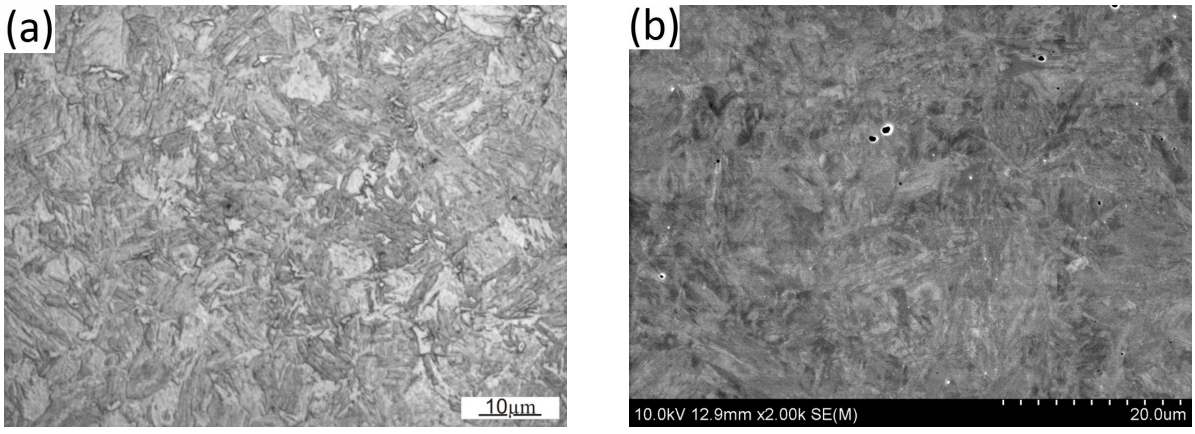

Fig. 7. The microstructure of steel sheet after stamping: (a) light microscopy (sample 1A); (b) SEM (sample 5), etched with 2 % nital

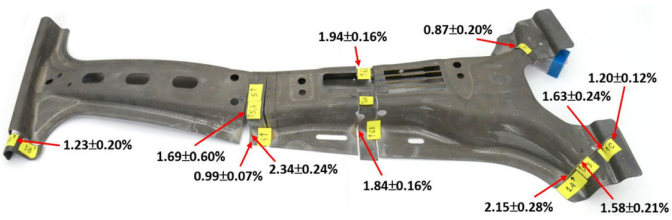

Fig. 8. Ferrite content in the microstructure of B pillar after hot stamping

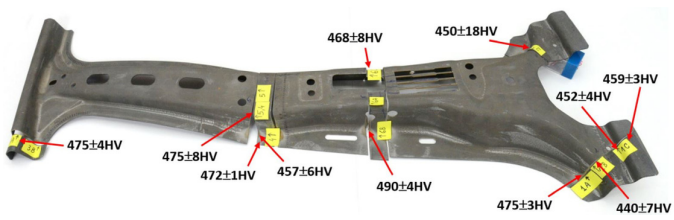

Fig. 9. Hardness (HV10) of B pillar after hot stamping. Measurements performed on the cross-sections

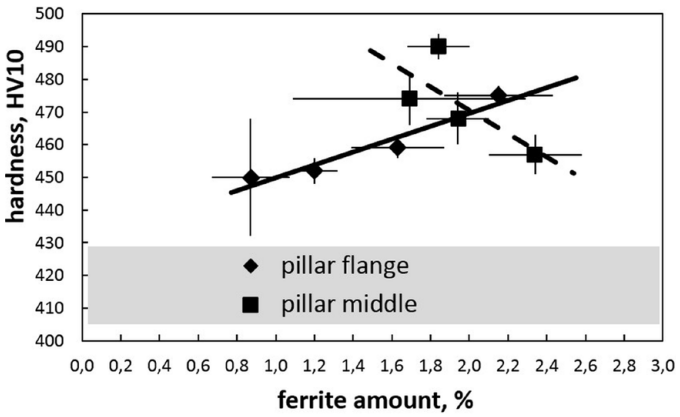

Fig. 10. Relationship between ferrite content and hardness

3.2. Strain analysis

The results of the simulation are presented in Fig. 11 and 12. Fig. 11 shows the stages of the B pillar forming process, reflecting the manufacturing stages described above (Fig. 3). Pam-Stamp 2G software postprocessor makes it possible to obtain maps of the distribution of plastic strain, represented by two in-plane components, ε_1 and ε_2. This allowed to generate the major strain and minor strain distribution maps, shown in Fig. 12, together with plotted forming limit curve (FLC), which made it possible to evaluate the risk of over-thinning or fracturing of a steel sheet.

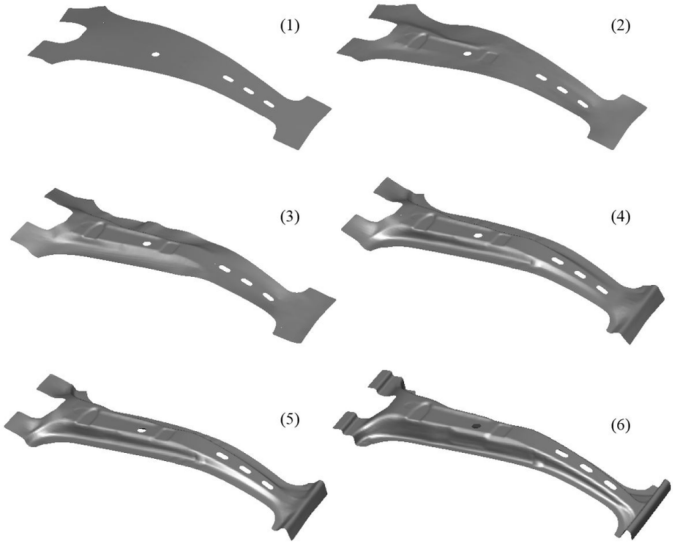

Fig. 11. Stages of B pillar forming as generated in numerical simulation using Pam-Stamp 2G

In order to verify the results of numerical analysis, the measurements of sheet thickness in different sections of a drawing piece were made (Fig. 4b). The results of measurements, compared with simulation, are presented in Fig. 13. As can be seen, good qualitative correspondence occurs considering the location of critical areas showing the largest thickness changes. However, a certain quantitative discrepancy can be observed, which may result from giving no consideration to normal anisotropy of a material at high temperature, in the simulation.

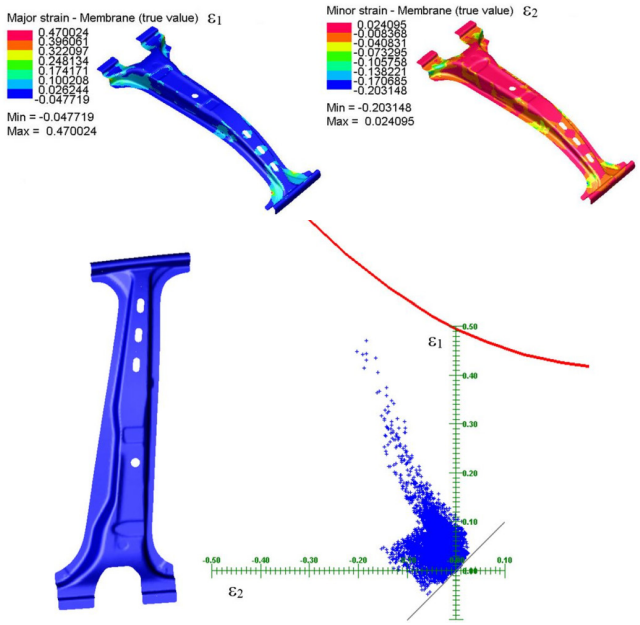

Fig. 12. Distribution of major and minor in-plane strains with plotted FLC

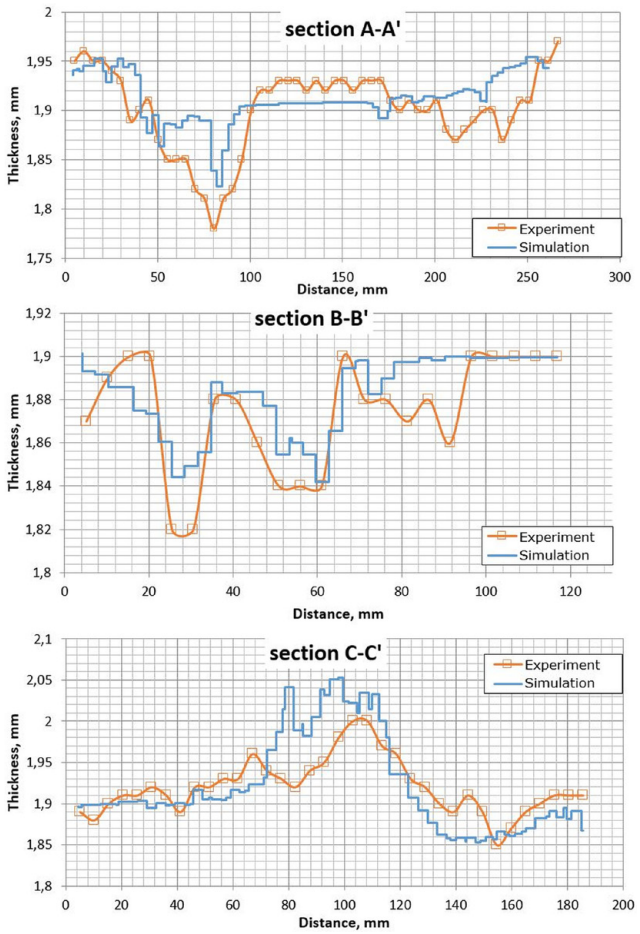

Fig. 13. Comparison of sheet thickness measurements with the results of simulation

4. Conclusions

The following conclusions can be drawn on the basis of this study:

1) The microstructure of the steel sheet in as-received condition consisted of ferrite and spheroidite. After hot stamping, it was expected to be fully martensitic. However, it transformed into martensite, bainite, and a small amount (2 %) of ferrite. It may be concluded that, due to the complexity of the shape of the drawn part, the cooling rate was not appropriate and non-uniform over the entire length of the part.
2) There was no simple correlation between the increase of ferrite content in the microstructure and hardness. There was also no clear correlation between ferrite content and amount of strain. Further research should be planned to investigate the interdependencies between these factors.
3) Before hot stamping, Al-Si protective layer has a diffusion sublayer Al-Fe-Si, which was formed by the diffusion of Fe from base material (steel) to surface layer. Although the microstructure of protective coating underwent substantial changes after hot stamping, the coating remained on the surface of B pillar after processing. However, the applied coating only inhibited the oxidation of iron and decarburization of steel sheet.
4) Numerous defects (cracks, pores) in the microstructure of the surface layer of the analyzed part before hot stamping were observed. Cracks are located perpendicular to the surface of the steel sheet. Porosity was observed in a layer between coating and base material (steel).
5) Analysis of simulation of sheet thickness distribution after hot stamping allows to identify dangerous areas in a drawing piece, where the loss of stability may take place. Thickness distribution obtained from numerical calculations testifies for a relatively safe process proceeding, in spite of quite complex draw piece geometry, which is an important advantage of hot stamping technology. The results of the simulation showed good qualitative coincidence with experimental data. The observed slight quantitative discrepancy may result from giving no consideration to normal anisotropy of a material at high temperature, in the simulation.

Acknowledgements

The authors are grateful to Kacper Ogłoza for his help in the realization of these investigations. Financial support of the Polish Ministry of Science and Higher Education is gratefully acknowledged (AGH-UST research project no. 16.16.110.663).

REFERENCES

[1] H. Karbasian, A.E. Tekkaya, Journal of Materials Processing Technology **210** (15), 2103-2118 (2010), https://doi.org/10.1016/j.jmatprotec.2010.07.019

[2] M. Löcker, K-MOBIL The Kirchhoff Group Magazine **16** (38), 6-9 (2011).

[3] N. Aziz, S.N. Aqida, IOP Conference Series: Materials Science and Engineering **50**, 012064 (2013), https://doi.org/10.1088/1757-899X/50/1/012064

[4] M. Huang, B. Wang, J. Zhou, X. Li, Procedia Engineering **81**, 1774-1779 (2014), https://doi.org/10.1016/j.proeng.2014.10.230

[5] H. Steinbeiss, H. So, T. Michelitsch, H. Hoffmann, Production Engineering – Research and Development **1** (2), 149-155 (2007), https://doi.org/10.1007/s11740-007-0010-3

[6] B.T. Tang, S. Bruschi, A. Ghiotti, P.F. Bariani, Finite Elements in Analysis and Design **81**, 69-81 (2014), https://doi.org/10.1016/j.finel.2013.11.009

[7] L. Zhu, Z. Gu, H. Xu, Y. Lu, J. Chao, Journal of Iron and Steel Research International **21** (2), 197-201 (2014), https://doi.org/10.1016/S1006-706X(14)60030-3

[8] J. Zhang, S. Jiang, Q. Zhang, C. Liu, Journal of Iron and Steel Research International **23** (3), 270-275 (2016), https://doi.org/10.1016/S1006-706X(16)30044-9

[9] S.J. Yao, L. Feng, D.L. Yang, D.X. Han, Y. Liu, Q.Q. Li, J.H. Guo, B.J. Chao, Journal of Materials Processing Technology **254**, 100-107 (2018), https://doi.org/10.1016/j.jmatprotec.2017.11.037

[10] M. Naderi, M. Ketabchi, M. Abbasi, W. Bleck, Procedia Engineering **10**, 460-465 (2011), https://doi.org/10.1016/j.proeng.2011.04.078

[11] B.A. Behrens, J. Schrödter, Numerical simulation of phase transformation during the hot stamping process, in: Proc. 5th International Conference on Thermal Process Modeling and Computer Simulation (2014).

[12] K. Liu, Y. Zhang, J. Mo, L. Jian, Applied Mechanics and Materials **378**, 397-402 (2013), https://doi.org/10.4028/www.scientific.net/AMM.378.397

[13] J. Min, J. Lin, L. Xin, J. Li, Advanced Materials Research **314-316**, 703-708 (2011), https://doi.org/10.4028/www.scientific.net/AMR.314-316.703

[14] J. Chen, X. Li, X. Han, in: S. Hashmi (Ed.), Comprehensive materials processing, Volume 5: Casting, semi-solid forming and hot metal forming, Elsevier, Amsterdam, 351-370 (2014).

[15] H.H. Bok, M.G. Lee, E.J. Pavlina, F. Barlat, H.D. Kim, International Journal of Mechanical Sciences 53 (9), 744-752 (2011), https://doi.org/10.1016/j.ijmecsci.2011.06.006

[16] Y. Chang, C.Y. Wang, K.M. Zhao, H. Dong, J.W. Yan, Materials and Design **94**, 424-432 (2016), https://doi.org/10.1016/j.matdes.2016.01.048

[17] X. Li, Y. Chang, C. Wang, P. Hu, H. Dong, Materials Science & Engineering A **679**, 240-248 (2017), https://doi.org/10.1016/j.msea.2016.10.045

[18] R. George, A. Bardelcik, M.J. Worswick, Journal of Materials Processing Technology **212**, 2386-2399 (2012), https://doi.org/10.1016/j.jmatprotec.2012.06.028

[19] M. Kumar, N. Sotirov, F. Grabner, R. Schneider, G. Mozdzen, Transactions of Nonferrous Metals Society of China **27**, 1257-1263 (2017), https://doi.org/10.1016/S1003-6326(17)60146-8

[20] Y. Chang, S. Li, X. Li, C. Wang, P. Hu, K. Zhao, Applied Thermal Engineering **99**, 419-428 (2016), https://doi.org/10.1016/j.applthermaleng.2016.01.053